Elastic scattering analysis of $^{16}O+^{208}Pb$ at 793 and 1503 MeV: Test of the closure approximation model

J. C. Pacheco,[1] M. D. Kadi-Hanifi,[2] and B. Bilwes[3]
[1]*Departamento de Física Aplicada e Instituto de Física Corpuscular, Centro Mixto CSIC Universitat de Valencia, E-46100 Burjassot, Valencia, Spain*
[2]*Institut des Sciences Exactes, Départment de Physique, Université de Blida, Blida, Algeria*
[3]*Institut de Recherches Subatomiques, IReS-IN2P3 BP28, F-67037 Strasbourg Cedex 2, France*
(Received 16 April 1999; published 23 August 1999)

Starting from a semiphenomenological analysis of the $^{16}O+^{208}Pb$ elastic scattering data at energies ranging from 78 to 312.6 MeV and using the dispersion relation, we have obtained the energy dependence of the real potential up to 1503 MeV. This real potential was then used with an absorptive potential calculated with a microscopic model, to analyze the elastic scattering at 793 and 1503 MeV. A good agreement between calculated and measured elastic scattering cross sections at 793 MeV corroborates that at this energy the collision is still dominated by collective processes. However, at 1503 MeV, the agreement between theoretical calculations and experiment is poor as expected, showing that the low collective modes are not the ''preponderant'' channels responsible for absorption anymore. [S0556-2813(99)01109-7]

PACS number(s): 25.70.Bc, 24.10.−i

I. INTRODUCTION

For many years, the optical model has been a useful tool to describe heavy ions elastic scattering. Particularly, the $^{16}O+^{208}Pb$ system has been widely studied because it is, from a theoretical point of view, an interesting system formed by two colliding spherical shell closed nuclei. Phenomenological Woods-Saxon potentials [1] as well as semiphenomenological ones, where the real part was deduced from renormalized double folding M3Y effective interaction [2], have been successfully used to reproduce the elastic scattering data in a large domain of energies ranging from 78 to 1503 MeV [1,2]. Assuming a semiclassical approach, theoretical calculations were carried out to evaluate the contribution to the imaginary potential coming from some of the lowest inelastic and transfer channels [3]. In the same way but starting from the Feshbach theory of the optical potential [4], different attempts were performed to evaluate the nucleus-nucleus potential. Both microscopic [5] and macroscopic [6] form factors were used to evaluate the contribution of some of the low lying inelastic channels to the potential. The nonelastic channels were introduced either individually [5–7] or globally [8], by assuming closure relations for both projectile and target nuclei. This last model calculates the contribution to the potential coming from all the collective inelastic channels and simulates the contribution due to transfer channels [9]. Within this model, elastic scattering data were reproduced successfully on a wide domain of energies that, in the case of $^{16}O+^{208}Pb$, ranges from 78 to 312.6 MeV [9,10]. It has also been used successfully to predict excitation functions of near- and sub-barrier fusion for $^{16}O+^{208}Pb$ and $^{32}S+^{40}Ca$ systems [10]. However, it should be valid for low energy scattering only and we are interested in this paper by studying its limits in terms of energy.

As we have previously shown for energies close to the Coulomb barrier, the radial distribution of the absorption is concentrated in a narrow domain of the nucleus surface potential. Considering only the contribution of the low lying inelastic channels [11] plus other peripheral processes (i.e., transfer) [12] one can reproduce the experimental data. When energy increases, the radial domain of the absorption broadens [11,13] and one cannot reproduce the elastic scattering data by taking into account only peripheral processes. Other nonelastic processes, such as nucleon-nucleon scattering, will also contribute to the absorption.

The closure approximation model would not be able to reproduce the elastic scattering data when energy increases if other processes not included in the model contribute significantly to the absorption. The aim of the present paper is to determine its validity at energies higher than those usually considered, where its predictive power has been widely tested. The model is better adapted to the calculations of the absorption than to the real potential mainly because of some intermediate approximations such as the use of a zero range n-n interaction. We will first determine the real potential in the semiphenomenological way presented in Sec. II, where we also determine its energy dependence with the help of the dispersion relation [14]. In Sec. III we briefly recall the model and its parameters. Elastic scattering cross section calculations at 793 and 1503 MeV will be shown and discussed in Sec. IV, while Sec. V is devoted to our conclusions.

II. ELASTIC SCATTERING ANALYSIS: ENERGY DEPENDENCE

Elastic scattering data of $^{16}O+^{208}Pb$ at energies listed in Table I, have been taken from Ref. [15] and analyzed in the same semimicroscopic way as in Ref. [2]. The absorptive part is chosen to be an energy dependent Woods-Saxon potential with parameters taken from Ref. [16]. They are given in Table I. The real part of the potential has been calculated as a double folding M3Y potential. The only difference with calculations of Refs. [2,16] is the ground state density which

TABLE I. $^{16}O+^{208}Pb$ semiphenomenological optical model parameters.

E_{lab} (MeV)	$N(E)$	W_0 (MeV)	rw (fm)	aw (fm)	$-V(12.4\,fm)$ (MeV)	$-W(12.4\,fm)$ (MeV)	σ_R (mb)	χ^2/n
78.00	1.726	28.350	1.2635	0.4206	2.859	0.456	40.30	0.7
80.00	1.479	29.590	1.2695	0.4408	2.450	0.641	109.30	1.2
81.00	1.581	32.280	1.2666	0.4201	2.618	0.549	140.20	1.3
82.00	1.635	29.809	1.3482	0.3077	2.708	1.063	205.50	0.4
83.00	1.606	26.760	1.3428	0.3211	2.659	0.950	253.80	1.0
85.95	1.414	27.436	1.3284	0.3847	2.342	1.214	451.90	1.0
87.00	1.429	29.380	1.3251	0.3730	2.366	1.104	475.60	0.9
88.00	1.380	25.476	1.3208	0.3681	2.285	0.835	495.80	1.3
90.00	1.266	32.953	1.2924	0.4339	2.097	1.039	626.80	0.7
94.00	1.112	35.300	1.2787	0.4840	1.842	1.245	842.30	1.7
96.00	1.259	32.240	1.2900	0.4424	2.085	1.037	894.30	0.5
102.00	1.000	36.150	1.2286	0.5687	1.656	0.999	1153.00	0.7
104.00	1.311	32.800	1.3099	0.4088	2.171	1.197	1208.00	0.2
129.50	1.100	35.578	1.2370	0.6271	1.822	1.511	2079.00	0.6
138.50	0.958	40.203	1.2155	0.6029	1.586	1.132	2152.00	3.1
192.00	0.952	42.223	1.2098	0.6196	1.577	1.209	2893.00	1.1
216.60	0.584	38.092	1.1595	0.7363	0.967	1.071	3069.00	1.5
312.60	0.868	23.783	1.2178	0.6478	1.437	0.874	3419.00	0.1

in our calculations is parametrized as a four parameter Fermi distribution:

$$\rho_c(r)=\rho_0(1+\omega r^2/c^2)\{1+\exp[(r-c)/z]\}^{-n}, \qquad (1)$$

where the ^{208}Pb, density was obtained in a variational semiclassical method [17] with $\omega=0.0$, $c=7.194$ fm, $a=0.658$ fm, $n=1.56$ for neutrons and $\omega=0.0$, $c=6.375$ fm, $a=0.535$ fm, $n=1.42$ for protons, while the ^{16}O density was obtained by fitting electron scattering data [18] with $\omega=-0.051$, $c=2.608$ fm, $a=0.513$ fm, $n=1$. For the ^{16}O nucleus, corrections due to the neutron charge distribution and finite proton range have been taken into account in the standard way [19]. We renormalize the bare real potential by fitting the experimental measurements with the help of the ECIS94 code [20]. The energy dependent renormalization factors are shown in Table I.

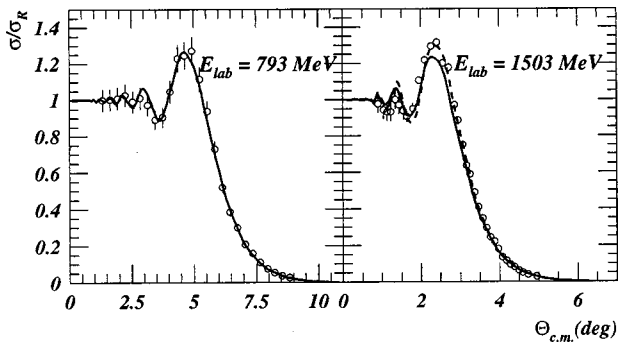

FIG. 1. Comparison of $^{16}O+^{208}Pb$ elastic scattering data with calculations. On the left we compare elastic scattering calculations with parameters of Mermaz *et al.* (full line) to our microscopic potentials at 793 MeV (full line). On the right we compare similar calculations with potentials of Eq. (4) (dashed line) to our microscopic ones at 1503 MeV (full line).

Elastic scattering data for $^{16}O+^{208}Pb$ at 793 MeV have been taken from Ref. [21]. Phenomenological calculations have been performed by using the optical model parameters of Mermaz *et al.* taken from Ref. [1]:

$$V_0=50\,\text{MeV}, \quad r_v=1.083\,\text{fm}, \quad a_v=0.755\,\text{fm},$$

$$W_0=42.2\,\text{MeV}, \quad r_w=1.083\,\text{fm}, \quad a_w=0.755\,\text{fm}. \qquad (2)$$

A good agreement between elastic scattering calculations and data is observed in Fig. 1(left). The σ_R and χ^2/n values are included in Table II.

At 1503 MeV elastic scattering data have been taken from Ref. [22]. In Eq. (3) we give the optical model parameters of Roussel *et al.* [1,23] used in optical model calculations:

$$V_0=80\,\text{MeV}, \quad r_v=1.072\,\text{fm}, \quad a_v=0.718\,\text{fm},$$

$$W_0=51.6\,\text{MeV}, \quad r_w=1.072\,\text{fm}, \quad a_w=0.718\,\text{fm}. \qquad (3)$$

TABLE II. $^{16}O+^{208}Pb$ elastic scattering and total reaction cross section calculations.

E_{lab} (MeV)	Real pot.	Im. pot.	$\sigma_R\,(mb)$	χ^2/n
793	Eq. (2)	Eq. (2)	3600	0.75
793	$N(793)\cdot V_{M3Y}$	Eq. (2)	3600	0.78
793	$N(793)\cdot V_{M3Y}$	Eq. (12)	3673	0.68
1503	Eq. (3)	Eq. (3)	3586	54.00
1503	Eq. (4)	Eq. (4)	3209	2.18
1503	$N(1503)\cdot V_{M3Y}$	Eq. (4)	3210	2.76
1503	$N(1503)\cdot V_{M3Y}$	Eq. (12)	3527	11.50

However, a bad agreement with the data was obtained by using these parameters in our calculations, as it is shown in Table II.

Keeping the same geometry for both real and imaginary potentials we searched for the depths of the real and imaginary potentials to reproduce the experimental measurements. We obtained

$$V_0 = 44\ \text{MeV}, \quad r_v = 1.072\ \text{fm}, \quad a_v = 0.718\ \text{fm},$$

$$W_0 = 26.1\ \text{MeV}, \quad r_w = 1.072\ \text{fm}, \quad a_w = 0.718\ \text{fm}. \quad (4)$$

Elastic scattering calculations with potentials of Eq. (4) are shown (dashed line) in Fig. 1 (right) and compared to experiments. In Table II we show the σ_R and χ^2/n values which are very different from those obtained using the parameters of Roussel of Eq. (3).

Energy dependence of the real potential has been experimentally observed [24,25] and theoretically well understood [10,14,26]. This phenomenon arises from the coupling between the elastic and nonelastic channels.

The energy dependence of the real potential is then related to the strength of these couplings and it is directly linked, by a dispersion relation, to the variation of the absorption with energy. The subtracted dispersion relation can be written as

$$\text{Re}\,\Delta V_{E_S}(r,E) = \frac{E-E_S}{\pi}\mathcal{P}\int_{E_0}^{\infty}\frac{\text{Im}\,\Delta V(r,E')}{(E'-E_S)(E'-E)}dE', \quad (5)$$

where $\mathcal{P}$ represents the principal value of the integral, E_0 is the threshold energy at which the imaginary potential vanishes, E_S is a reference energy, and $\text{Re}\,\Delta V_{E_S}(r,E)$ is given by

$$\text{Re}\,\Delta V_{E_S}(r,E) = V(r,E) - V(r,E_S), \quad (6)$$

where $V(r,E_S)$ is the value of our total real potential at the reference energy. This real potential can be calculated with Eq. (5).

In a linear schematic model [14,27] Eq. (5) can be evaluated assuming that $\text{Im}\,\Delta V(r,E')$ can be represented by linear segments joining the values of the imaginary potential as shown in Fig. 2 (bottom). We have chosen four segments consistent with the values of $W(r)$ at $r = 12.4$ fm, deduced from the elastic scattering analysis of Refs. [1,2] and Eqs. (2) and (4), and plotted in Fig. 2 as a function of laboratory energy E_{lab}. The segments connect the values $-W(r = 12.4\ \text{fm}) = 0,1.21,0.84,0.56,0.24$ MeV corresponding to $E_{\text{lab}} = 74$, 85.95, 400, 793, and 1503 MeV, respectively. We then obtain, for a given radius, the energy dependence of the real potential which can be expressed as an energy dependent renormalization factor $N(E)$. Following Ref. [14] calculations have been carried out assuming an average sensitivity radius of 12.4 fm and a reference energy of 138.5 MeV. In Fig. 2 (top) we compare the values of the potentials obtained at 12.4 fm with Eq. (5), to those deduced from the fit of the elastic scattering data which are included in Table I. A good agreement is observed. Since in this paper we are interested by higher energies and we need the real potential to calculate

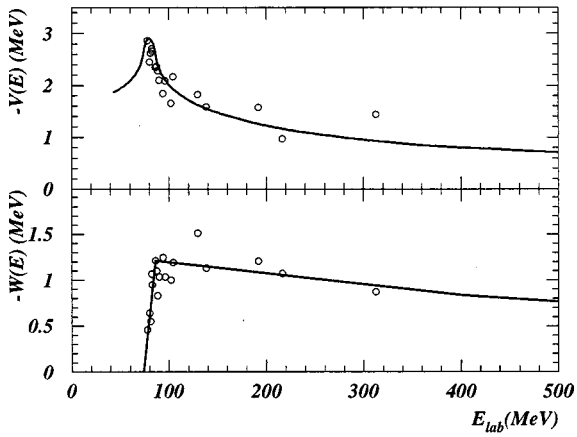

FIG. 2. Energy dependence of the real potential for $^{16}O+^{208}Pb$ at 12.4 fm.

our microscopic absorptive potential, we use the dispersion relation to obtain $N(793\ \text{MeV}) = 0.331$ and $N(1503\ \text{MeV}) = 0.255$. When energy increases it is known that the sensitivity radius decreases and the sensitivity domain of the imaginary potential broadens. We can expect a sensitivity radius shorter than 12.4 fm [23] at the highest energies and a sensitivity domain of the potential different from that of the lowest energies for which it is known to be very narrow [11]. We could construct a new dispersion relation at this shorter sensitivity radius but it would not have a physical meaning. Indeed, the energy dependence of the real potential is related to the energy dependence of the imaginary one, which strongly changes in the vicinity of the barrier, where the sensitivity domain of the potential is very narrow and surrounds 12.4 fm. Assuming at these energies, a sensitivity radius very different from 12.4 fm we get out of the sensitivity domain where the absorption takes place and the corresponding imaginary potential is unphysical.

We can verify that the real potential calculated from our dispersion relation with Eq. (5) shows a correct radial dependence. In Fig. 3 (left) we compare the real potential of Eq. (5) (bold full line) at 793 MeV to the real potential of Eq. (2) (bold dashed line). Starting from 10 fm they both agree. At 1503 MeV the agreement between the real potential deduced from Eq. (5) (full line) and that of Eq. (4) (dashed line) is observed starting from 9.5 fm. This figure also shows that the energy dependences of the renormalized real potentials of Eq. (5) and that of the phenomenological ones of Eqs. (2) and (4) are roughly the same. These results give support to our dispersion relation and justify the use of the renormalized potentials in the following calculations.

III. THE MODEL: MICROSCOPIC ABSORPTIVE POTENTIAL CALCULATIONS

The closure approximation model [7] starts from the Feshbach theory [4] where the nonlocal optical potential is given by

$$V(\mathbf{r},\mathbf{r}') = U_0(\mathbf{r})\,\delta(\mathbf{r}-\mathbf{r}') + \Delta V(\mathbf{r},\mathbf{r}') = U_0(\mathbf{r})\,\delta(\mathbf{r}-\mathbf{r}') + \text{Re}\,\Delta V(\mathbf{r},\mathbf{r}') + i\,\text{Im}\,\Delta V(\mathbf{r},\mathbf{r}')\,. \quad (7)$$

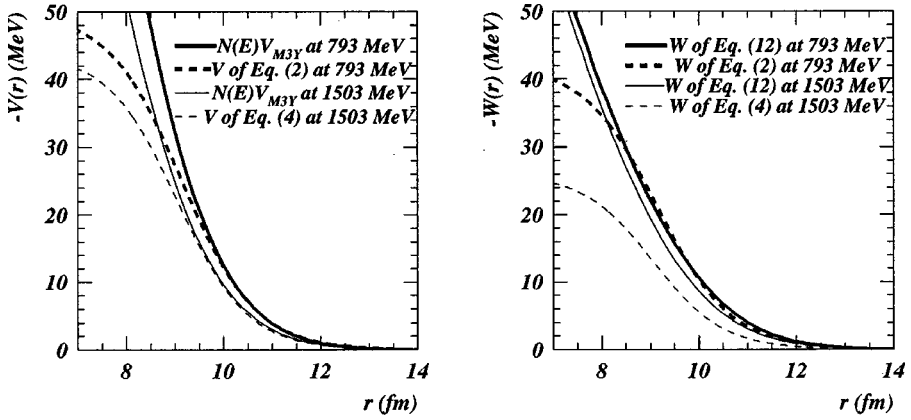

FIG. 3. Microscopic and phenomenological potentials for $^{16}O+^{208}Pb$. On the left, the renormalized real potentials of Eq. (5) at 793 MeV (bold full line) and at 1503 MeV (full line) are compared to the phenomenological ones of Eqs. (2) (bold dashed line) and (4) (dashed line), respectively. On the right, our microscopic imaginary potentials at 793 MeV (bold full lines) and at 1503 MeV (full line) are compared to the phenomenological ones of Eqs. (2) (bold dashed line) and (4) (dashed line), respectively.

Although the model evaluates the total potential of Eq. (7), we are only interested in the absorptive part which, in the weak coupling limit, can be written as

$$\mathrm{Im}\,\Delta V(\mathbf{r},\mathbf{r}') = \sum_{(m,n)\neq(0,0)} V^{*}_{m,n}(\mathbf{r})\,\mathrm{Im}\,G_{m,n}(\mathbf{r},\mathbf{r}')\,V_{m,n}(\mathbf{r}'), \tag{8}$$

where $\mathrm{Im}\,G_{m,n}(\mathbf{r},\mathbf{r}')$ is the imaginary part of the relative motion propagator in channel (m,n) and $V_{m,n}(\mathbf{r})$ is the transition matrix element from the initial state (where target and projectile are in their ground states) to the intermediate state (where at least one of the two nuclei is excited). Equation (8) can be evaluated by assuming a number of simplifying hypotheses.

(1) The $G_{m,n}$ propagator is approximated by the WKB propagator

$$G_{m,n}(\mathbf{r},\mathbf{r}') \simeq G^{\mathrm{WKB}}_{m,n}(\mathbf{r},\mathbf{r}'). \tag{9}$$

(2) Assuming that all excited states are concentrated in a narrow domain of energy one can replace their excitation energies by average values $(\overline{E}_T)$ for the target and $(\overline{E}_P)$ for the projectile. Under this assumption, the WKB propagator is replaced by an average WKB propagator for each one of the two colliding nuclei:

$$G^{\mathrm{WKB}}_{m,n}(\mathbf{r},\mathbf{r}') \simeq \overline{G}^{\mathrm{WKB}}_{i}(\mathbf{r},\mathbf{r}'), \quad i=1,2,3. \tag{10}$$

In this way, Eq. (8) only includes three terms that describe the excited states of each one $(m\neq 0, n=0)$, $(m=0, n\neq 0)$ or both $(m\neq 0, n\neq 0)$ of the two colliding nuclei, which corresponds to $i=1,2,3$, respectively.

(3) If the closure relation on complete sets of m (projectile) and n (target) states is introduced in Eq. (8), all nonelastic channels are implicitly taken into account.

(4) A separable two body interaction [28] with Gaussian form factors is assumed. This effective force can be written as

$$v_{ij}(\mathbf{r}) = -V_0 \exp\left[-\frac{\mu}{2}(\mathbf{r}_i+\mathbf{r}_j)^2\right]\exp\left[-\frac{\mu}{2}(\mathbf{r}_i-\mathbf{r}_j+\mathbf{r})^2\right], \tag{11}$$

where μ is a parameter related to the r_0 interaction range, $r_0=(2/\mu)^{1/2}$, and V_0 is the strength of the interaction.

(5) The Slater approximation [29] is assumed to describe the off diagonal elements of the density matrix.

(6) If the nonlocality range of the potential of Eq. (8) is small in comparison with the range of the potential U_0 of Eq. (7), the local imaginary potential can be approximated by the first term of the Wigner transform [30] of the nonlocal potential. In this way our imaginary local potential is finally given by

$$\mathrm{Im}\,\Delta V(R) = \int_0^{\infty} e^{i\mathbf{k}\cdot\mathbf{s}}\,\mathrm{Im}\,\Delta V(\mathbf{R},s)\,ds, \tag{12}$$

where $\mathrm{Im}\,\Delta V(\mathbf{R},s)$ is the nonlocal potential of Eq. (8) now expressed in terms of the center of mass and relative motion coordinates $\mathbf{R}$ and s, defined by $\mathbf{R}=(\mathbf{r}+\mathbf{r}')/2$ and $s=\mathbf{r}-\mathbf{r}'$. The details of the derivation of the local imaginary potential are given in Ref. [8]

The input parameters of the model are only the $\overline{E}_T$ and $\overline{E}_P$ average excitation energies of the two colliding nuclei, the strength, V_0, and range, r_0, parameters of the two body effective interaction and the ground state densities of the target and projectile. The values adopted here for these parameters are given in Refs. [9–12] where they have been widely tested. $\overline{E}_P$ and $\overline{E}_T$ were determined to be 6.5 and 3.5 MeV from the excitation spectrum of ^{16}O and ^{208}Pb, respectively. As we have shown in Ref. [9] this assumption reproduces well the absorption coming from the low-lying collective channels but overestimates the absorption due to the contribution of the high-lying collective channels in a way that decreases when energy increases. In Ref. [9] we also discuss how in the closure approximation model the high-lying states are taken into account to simulate transfer contributions. Indeed, our imaginary potential contains much

more than only the contribution coming from low- and high-lying channels. Due to the inclusion of the closure relations all mean-field excitations are implicitly included. However, the nucleon-nucleon scattering channels are not taken into account by the model. The strength and range were fixed to be $V_0=58.7$ MeV and $r_0\simeq 2$ fm. While the value of the strength is very close to those obtained for different systems [9,10,31,32], the range of the interaction is ~24% larger than the 1.69 fm assumed for all the analyzed systems. In Ref. [8] it is shown why for strongly asymmetric systems the range of the separable two body interaction must be larger than it is for symmetric ones. The ground state densities used in matrix element calculations have previously been given in Sec. II. Finally, to evaluate the average WKB propagator of Eq. (10) and then calculate the imaginary local potential of Eq. (12), the renormalized real potential deduced from Eq. (5) has been used.

Microscopic absorptive potentials have been calculated at 793 and 1503 MeV with Eq. (12). In Fig. 3 (right) these potentials are shown and compared to the phenomenological ones obtained from Eqs. (2) and (4), respectively. At 793 MeV an excellent agreement between the potentials calculated with Eq. (12) (bold full line) and Eq. (2) (bold dashed line) is observed from 8 fm. However, at 1503 MeV one can observe that the potential calculated from Eq. (12) (full line) has a longer range than the phenomenological one calculated from Eq. (4) (dashed line). This figure also shows different energy dependences of the imaginary potentials of Eq. (12) and of the phenomenological ones of Eqs. (2) and (4). One can give a qualitative explanation of these different energy dependences and different long range of the imaginary potentials calculated at 1503 MeV with Eqs. (4) and (12). Indeed, the closure approximation model evaluates the contribution to the imaginary potential due to the mean field excitations. Particularly the low-lying collective states and the transfer processes, simulated through the high-lying states, give a long range contribution to the absorptive potential whose energy dependence is only given by the one included in the WKB propagator. However, it is known that at high energies the nucleon-nucleon scattering becomes important giving a contribution to the volume part of the imaginary potential which exhibits a short range, while the combined effects of the energy dependence of the mean field and recoil gradually diminish the absorption due to transfer and inelastic processes. In Ref. [33] it is shown that at bombarding energies above 50 MeV/nucleon the absorption due to large-angle nucleon-nucleon scattering is not too important but clearly dominates above 150 MeV/nucleon. We can easily understand why our microscopic potential at 793 MeV (49.5 MeV/nucleon) agrees with the phenomenological one from 8 fm showing a similar range. Nevertheless, at 1503 MeV (93.9 MeV/nucleon) our microscopic potential disagrees with the phenomenological one and shows a different range. In fact, at 793 MeV the nucleon-nucleon scattering channels give a low contribution to the absorption which is dominated by the long range contribution due to the low-lying states which are included in our calculations. However at 1503 MeV the contribution to the absorption coming from the open nucleon-nucleon scattering channels is very important [33] while that of the low-lying states is strongly attenuated. This leads to a shorter range absorptive potential compared to the one calculated with the closure approximation model, where the imaginary potential is dominated by the long range terms coming from the low-lying channels contribution.

IV. CROSS SECTION CALCULATIONS AT 793 AND 1503 MeV

A previous phenomenological elastic scattering calculation at 793 MeV has been assumed as a reference to test our real potential deduced from Eq. (5). In fact, assuming the imaginary Woods-Saxon potential given in Eq. (2) and our real potential extracted from the dispersion relation, we calculate the elastic scattering and total reaction cross sections. Table II shows the σ_R and χ^2/n values which are very close to those obtained using the parameters of Mermaz given in Eq. (2). In Fig. 1 (left) we cannot distinguish between both calculations. This is a way to show that both the real potential of Mermaz *et al.* of Eq. (2) and our real potential deduced from Eq. (5) are equivalent. This equivalence as well as the good agreement observed in Fig. 3 (left) between both potentials of Eqs. (2) (bold dashed line) and (5) (bold full line) from 10 fm, show the insensitivity of the elastic scattering and cross section calculations to the value of the real potential at short distances. The sensitivity domain must be placed at distances larger than 10 fm. Finally, by using the renormalized double folding potential deduced from the dispersion relation in Sec. II and the microscopic absorptive potential calculated in the way described in Sec. III, elastic scattering distribution and total reaction cross section calculations are performed at 793 MeV. The σ_R and χ^2/n values included in Table II are very close to those calculated with phenomenological or semimicroscopic potentials. In Fig. 1 (left) we compare experiments and microscopic calculations (full line) which are indistinguishable from the previous ones. The very good agreement observed between calculations and data in all the angular domain where the elastic scattering cross sections have been measured, shows the equivalence between the imaginary potential of Eq. (2) and our microscopic absorptive term, as it is shown in Fig. 3 (right) where one can observe that both potentials agree from 8 fm. These agreements have a twofold meaning: the potential gives a negligible contribution to the absorption for distances lower than 8 fm and the model includes all the channels that contribute significantly to the absorption which starts from about 8 fm. Effectively, the total reaction cross section σ_R can be written as [12,34]

$$\sigma_R=\int_0^\infty f(r)dr \quad \text{with}$$

$$f(r)=-\frac{1}{(2I_P+1)(2I_T+1)}\sum_l \frac{8\pi}{k^2\hbar v_0} \times(2l+1)|\chi_l(r)|^2 W(r), \tag{13}$$

where I_P, I_T are the intrinsic spin of the projectile and target nuclei in their ground states, v_0, l, and $\chi_l(r)$ are the velocity,

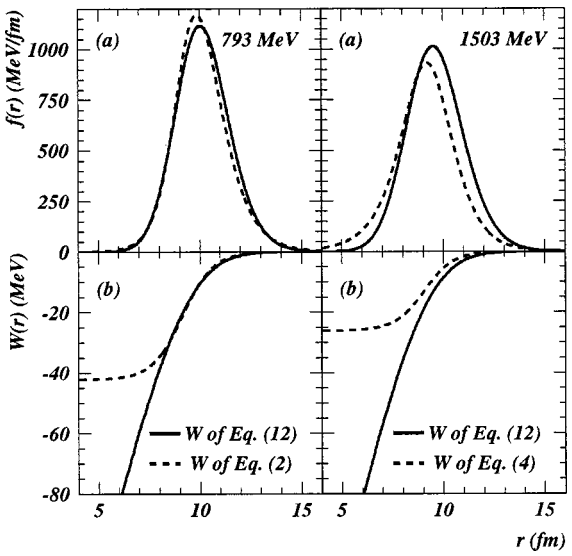

FIG. 4. On the left (a) we show the radial distributions of the absorption calculated from Eq. (13) at 793 MeV with the imaginary potentials of Eq. (12) (full line) and Eq. (2) (dashed line) which are drawn on the left (b) with the same symbols. On the right we show similar calculations at 1503 MeV.

angular momentum, and radial part of the partial wave function of the relative motion in the elastic channel at the $E_{\mathrm{c.m.}}$ energy, k is the wave number, and $W(r)$ is the absorptive potential.

The ECIS94 code [20] was used to calculate the $\chi_l(r)$ wave functions with the real potential extracted from the dispersion relation and the imaginary ones evaluated with Eqs. (2) and (12) at 793 MeV and Eqs. (4) and (12) at 1503 MeV. At 793 MeV the radial distribution of the absorption $f(r)$ has been calculated from Eq. (13). On the left of Fig. 4(a), calculations assuming the absorptive potential of Eq. (12) (full line) are shown and compared to the ones obtained with the phenomenological potential of Eq. (2) (dashed line). The value of the area under each curve corresponds to the total reaction cross section calculated with the imaginary potential of Eq. (12) (full line) and Eq. (2) (dashed line), respectively, that we draw in Fig. 4(b) (left). The agreement observed between both radial distributions is excellent and the total reaction cross sections differ by less than 2%.

In Figs. 5(a)–5(c) the $(2l+1)|\chi_l(r)|^2$ functions calculated at 793 MeV assuming as absorptive terms our microscopic potential (full line) and the one deduced from Eq. (2), are shown for some values of the l-angular momentum. The agreement is excellent. From Figs. 4(b) (left) and 5(a)–5(c) we can easily understand the shape of the radial distributions of the absorption and their agreement. Indeed, at distances shorter than 6 fm the negligible values of the $(2l+1)|\chi l(r)|^2$ functions [Figs. 5(a)–5(c)] annihilate the strong value of the imaginary potential. However, at distances larger than 15 fm the negligible value of the imaginary potential annihilates the strong values of the $(2l+1)|\chi_l(r)|^2$ functions and then the absorption is concentrated in the radial domain where both imaginary potentials of Eqs. (12) and (2) agree.

Following at 1503 MeV the same procedure as we did for 793 MeV we use the imaginary Woods-Saxon parameters of Eq. (4) and the real potential deduced from dispersion relation given by Eq. (5). We, then calculate the elastic scattering distribution and total reaction cross section. In Table II we show the σ_R and χ^2/n values which are very close to those calculated with potentials of Eq. (4). A good agreement between both calculations is shown in Fig. 1 (right) (dashed line) where they are indistinguishable. The equivalence between the real potential given in Eq. (4) and the one calculated from Eq. (5) is then evident. In Fig. 3 (left) one can observe that both potentials agree from 9.5 fm, showing the insensitivity of the calculations to the values of the real potential at short distances. Both phenomenological and semimicroscopic calculations have been taken as a reference for comparison with microscopic ones. Assuming this renormalized real potential and the microscopic absorptive term calculated in the way described in Sec. III, elastic scattering calculations performed at 1503 MeV give σ_R and χ^2/n values (Table II) which are very different from those calculated with phenomenological or semimicroscopic potentials. In Fig. 1 (right) we compare experimental measurements to microscopic calculations (full line). A poor agreement is observed. Our microscopic potential gives a total reaction cross section 10% greater than the one calculated with phenomenological or semimicroscopic potentials.

On the right of Fig. 4(a) we compare the radial distributions of the absorption calculated from Eq. (13) with the

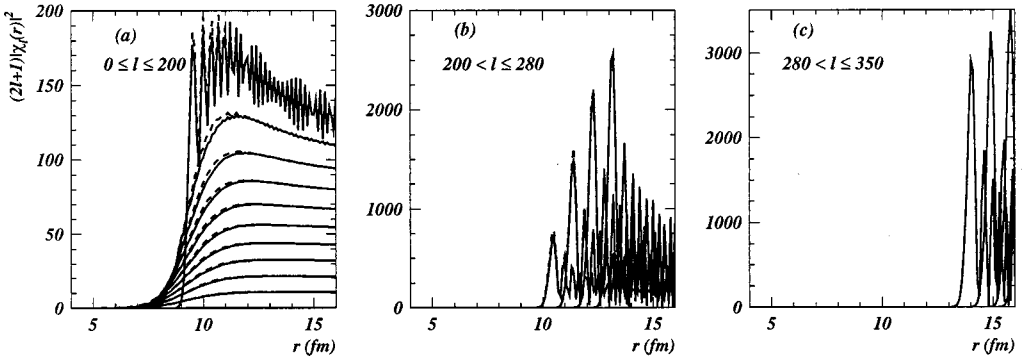

FIG. 5. Some of the $(2l+1)|\chi_l(r)|^2$ functions for the $^{16}O+^{208}Pb$ system at 793 MeV calculated with the imaginary potentials of Eq. (12) (full line) and Eq. (2) (dashed line).

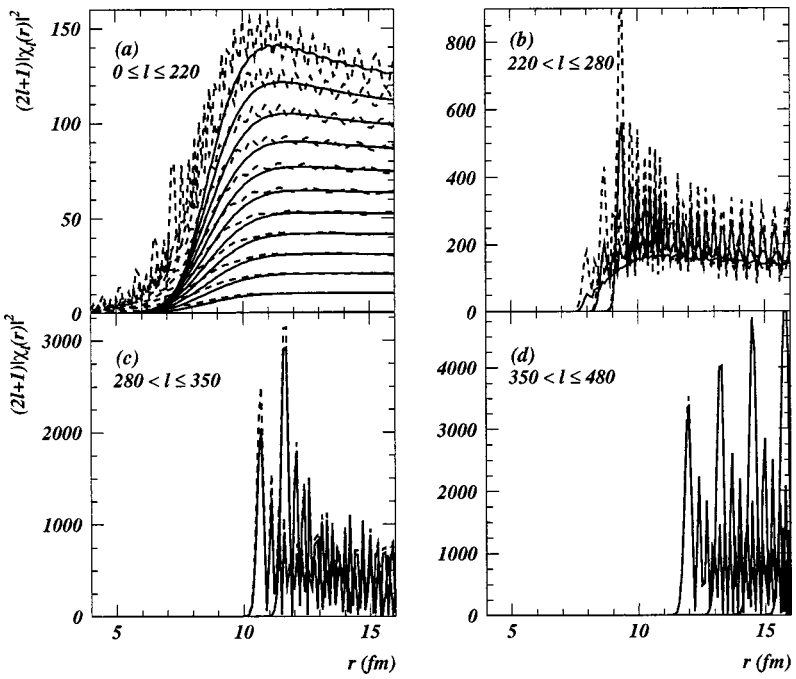

FIG. 6. Some of the $(2l+1)|\chi_l(r)|^2$ functions for the $^{16}O+^{208}Pb$ system at 1503 MeV calculated with the imaginary potentials of Eq. (12) (full line) and Eq. (4) (dashed line).

imaginary potentials of Eq. (12) (full line) and Eq. (4) (dashed line). The imaginary potential of Eq. (4) has been fitted to reproduce the data; it then, implicitly includes the absorption coming from all the open channels. As we have discussed in Sec. III, at this energy, the nucleon-nucleon scattering becomes very important and gives a strong contribution to the volume imaginary potential which exhibits a short range, while the low-lying state excitations gives a slight surface imaginary potential. When new channels are open the absorption is distributed among all the open channels and the shape of the imaginary potential changes. Indeed, the imaginary potential of Eq. (4) must show a shorter range than the microscopic one calculated from Eq. (12) which overestimates the low-lying state contributions and does not take into account the nucleon-nucleon scattering. On the right of Fig. 4(b) we show the imaginary potentials of Eq. (4) (dashed line) and Eq. (12) (full line). Both potentials strongly disagree in the domain of distances where the absorption takes place, being our microscopic potential stronger than the phenomenological one. In Fig. 6(a)–6(d) the $(2l+1)|\chi_l(r)|^2$ functions calculated at 1503 MeV with the imaginary potentials of Eqs. (12) (full line) and (4) (dashed line), are drawn for some values of the *l*-angular momentum. The most important contribution to the absorption comes from the functions with higher angular momentum which roughly agree for both potentials [Figs. 6(c) and 6(d)]. Indeed, the higher value of the total reaction cross section obtained with the potential of Eq. (12) is consistent with its higher strength in the sensitivity domain.

V. CONCLUSIONS

Starting from the imaginary Woods-Saxon potentials obtained from elastic scattering calculations performed at energies ranging from 78 to 312.6 MeV and assuming a very simple modelling of the subtracted dispersion relation, we calculate the energy dependence of the real potential up to 1503 MeV at an average sensitivity radius of 12.4 fm. Elastic scattering calculations performed at 793 and 1503 MeV are then consistent with the dispersion relation.

Optical model calculations have been performed at 793 MeV assuming the phenomenological imaginary potential of Eq. (2) and the real ones of Eqs. (2) and (5). Comparison between experimental measurements and elastic scattering calculations shows the equivalence between both real potentials which agree from 10 fm.

Assuming the real potential of Eq. (5), a microscopic absorptive potential has been calculated starting from the closure approximation model which globally evaluates the contribution to the absorption coming from all nonelastic channels of both target and projectile nuclei. This model has proved to be very successful in predicting experimental measurements and excitation functions at energies ranging from the Coulomb barrier up to 20 MeV/nucleon but has never been tested at much higher energies. Elastic scattering calculations performed with the real potential of Eq. (5) and the microscopic absorptive one are in very good agreement with data, showing that at 793 MeV the absorption is then mostly controlled by collective processes included in the model and consequently the model is able to reproduce the experimental measurements.

In the same way, optical model calculations at 1503 MeV have been performed assuming the absorptive potential of Eq. (4) and the real ones of Eqs. (4) and (5). A good agreement between experimental measurements and elastic scattering calculations was obtained showing the equivalence between both real potentials which agree from 9.5 fm.

Finally, elastic scattering calculations have been performed with the help of our microscopic absorptive potential. The disagreement observed between theoretical calculations and experimental measurements shows that the model is not able to reproduce the data. Indeed, at this energy deeper pro-

cesses, such as nucleon-nucleon scattering, become very important giving a short rage imaginary potential and the relative contribution to the absorption coming from the low-lying channels is strongly attenuated. The imaginary potential must then exhibit a shorter range than when nucleon-nucleon channels are not open. The closure approximation model does not take into account the nucleon-nucleon channels and overestimates the low-lying states contribution to the absorption. In fact, the model gives a too long range imaginary potential and, consequently, a too big total reaction cross section.

ACKNOWLEDGMENTS

The authors wish to express their gratitude to N. Vinh Mau for her stimulating discussions and criticisms. This work was partially supported by CICYT under Project No. AEN96-1662.

[1] F. Videbaeck, R. B. Goldstein, L. Grodzins, S. A. Steadman, T. A. Belote, and J. D. Garrett, Phys. Rev. C **15**, 954 (1977); S. C. Pieper, M. H. Macfarlane, D. H. Gloeckner, D. G. Kovar, F. D. Becchetti, B. G. Harvey, D. L. Hendrie, H. Homeyer, M. Mahoney, F. Pühlhofer, W. Von Oertzen, and M. S. Zisman, *ibid.* **18**, 180 (1978); C. Olmer, M. Mermaz, M. Buenerd, C. K. Gelbke, D. L. Hendrie, J. Mahoney, D. K. Scott, M. H. Macfarlane, and S. C. Pieper, *ibid.* **18**, 205 (1978); E. Vulgaris, L. Grodzins, S. G. Steadman, and R. Ledoux, *ibid.* **33**, 2017 (1986); M. C. Mermaz *et al.*, Z. Phys. A **326**, 353 (1987); J. B. Ball, C. B. Fulmer, E. E. Gross, M. L. Halbert, D. C. Hensley, C. A. Ludermann, M. J. Saltmarsh, and G. R. Satchler, Nucl. Phys. **A252**, 208 (1975); P. Roussel-Chomaz, N. Alamanos, F. Auger, J. Barrette, B. Berthier, B. Fernandez, L. Papineau, H. Doubre, and W. Mittig, *ibid.* **A477**, 345 (1988); I. J. Thompson, M. A. Nagarajan, J. S. Lilley, and M. J. Smithson, *ibid.* **A505**, 84 (1989); M. J. Smithson, J. S. Lilley, M. A. Nagarajan, P. V. Drumm, R. A. Cunningham, B. R. Fulton, and I. J. Thompson, *ibid.* **A517**, 193 (1990).

[2] J. S. Lilley, B. R. Fulton, M. A. Nagarajan, I. J. Thompson, and D. W. Banes, Phys. Lett. **151B**, 181 (1985); M. A. Nagarajan, C. Mahaux, and G. R. Satchler, Phys. Rev. Lett. **54**, 1136 (1985).

[3] R. A. Broglia, G. Pollarolo, and A. Winther, Nucl. Phys. **A361**, 307 (1981); **A406**, 369 (1983).

[4] H. Feshbach, Ann. Phys. (N.Y.) **5**, 357 (1958); **19**, 287 (1962).

[5] M. A. Andrés, F. Catara, and F. G. Lanza, Inst. Phys. Conf. Ser. **110**, 231 (1990); Phys. Rev. C **44**, 2709 (1991).

[6] K. I. Kubo and R. E. Hodgson, Nucl. Phys. **A366**, 310 (1981).

[7] W. G. Love, T. Terasawa, and G. R. Satchler, Nucl. Phys. **A291**, 183 (1977); Z. El-Itaoui, P. J. Ellis, and B. A. Mugharabe, *ibid.* **A441**, 511 (1985); K. I. Kubo, *ibid.* **A534**, 381 (1991).

[8] N. Vinh Mau, Nucl. Phys. **A457**, 413 (1986); **A470**, 406 (1987); Inst. Phys. Conf. Ser. **110**, 1 (1990).

[9] N. Vinh Mau, J. L. Ferrero, J. C. Pacheco, and B. Bilwes Nucl. Phys. **A531**, 435 (1991); Phys. Rev. C **47**, 899 (1993); M. V. Andrés, F. Catara, and E. Lanza, *ibid.* **47**, 902 (1993).

[10] N. Vinh Mau, J. C. Pacheco, J. L. Ferrero, and B. Bilwes, Nucl. Phys. **A560**, 879 (1993).

[11] J. C. Pacheco, B. Bilwes, F. Sánchez, J. A. Ruíz, J. Díaz, J. L. Ferrero, and M. D. Kadi-Hanifi, Nucl. Phys. **A588**, 537 (1995).

[12] J. C. Pacheco, M. D. Kadi-Hanifi, B. Bilwes, and F. Remiro, Phys. Rev. C **59**, 1518 (1999).

[13] M. D. Kadi-Hanifi, Thèse d'état, Université d'Alger, 1999.

[14] C. Mahaux, H. Ngô, and G. R. Satchler, Nucl. Phys. **A449**, 354 (1986); **A456**, 134 (1986).

[15] J. Lilley (private communication).

[16] M. A. Nagarajan (private communication).

[17] M. Brack, C. Guet, and R. B. Hakansson, Phys. Rep. **123**, 274 (1985).

[18] I. Sick and J. S. Mc Carthy, Nucl. Phys. **A150**, 631 (1979).

[19] G. R. Satchler and W. G. Love, Phys. Rep. **55**, 183 (1979).

[20] J. Raynal, Nuclear Data Bank of the OCDE, 1994 (unpublished).

[21] I. Linck (private communication).

[22] P. Roussel (private communication).

[23] P. Roussel, Thèse d'état, Université Paris-Sud, Centre d'Orsay, 1986.

[24] A. Baeza, B. Bilwes, R. Bilwes, J. Díaz, and J. L. Ferrero, Nucl. Phys. **A419**, 412 (1984).

[25] J. Díaz, J. L. Ferrero, J. A. Ruíz, B. Bilwes, and R. Bilwes, Nucl. Phys. **A494**, 311 (1989).

[26] J. C. Pacheco, J. L. Ferrero, N. Vinh Mau, and B. Bilwes, Phys. Lett. B **267**, 455 (1991).

[27] B. Bilwes, R. Bilwes, F. Ballester, J. Díaz, J. L. Ferrero, C. Roldán, L. Stuttgé, and F. Sánchez, Nucl. Phys. **A473**, 353 (1987).

[28] G. E. Brown and M. Bosterli, Phys. Rev. Lett. **3**, 472 (1959); A. Bohr and B. R. Mottelson, *Nuclear Structure* (Benjamin, New York, 1975).

[29] A. B. Santra and B. Shina, Phys. Lett. **110B**, 359 (1982).

[30] F. G. Perey and B. Buck, Nucl. Phys. **32**, 363 (1962); R. Peierls and N. Vinh Mau, *ibid.* **A343**, 1 (1980); F. G. Perey and D. S. Saxon, Phys. Lett. **10**, 107 (1964); H. Horinchi, Prog. Theor. Phys. **64**, 184 (1980).

[31] J. L. Ferrero, J. C. Pacheco, A. Baeza, J. M. Barrigón, B. Bilwes, R. Bilwes, and N. Vinh Mau, Nucl. Phys. **A514**, 367 (1990); B. Bilwes, R. Bilwes, N. Vinh Mau, J. L. Ferrero, and J. C. Pacheco, *ibid.* **A526**, 292 (1991); J. M. Barrigón, A. Baeza, J. L. Ferrero, J. C. Pacheco, B. Bilwes, and R. Bilwes, *ibid.* **A545**, 720 (1992).

[32] J. M. Barrigón, Tesis Doctoral, Universidad de Extremadura, 1991.

[33] J. H. Sörensen and A. Winther, Nucl. Phys. **A550**, 329 (1992).

[34] G. R. Satchler, *Direct Nuclear Reactions* (Oxford University Press, New York, 1983).